

Review

# Effect of 3D-Printed Porous Titanium Alloy Pore Structure on Bone Regeneration: A Review

Si He <sup>†</sup>, Jiang Zhu <sup>†</sup>, Yiwan Jing, Shuai Long , Lu Tang, Lijia Cheng <sup>\*</sup>  and Zheng Shi <sup>\*</sup>

Clinical Medical College & Affiliated Hospital, School of Basic Medical Sciences, Mechanical Engineering College, Chengdu University, Chengdu 610106, China; hesisi0420@163.com (S.H.); 13378119012@163.com (J.Z.); m18380728911@163.com (Y.J.); 11319288735@gmail.com (S.L.); tl20120613@163.com (L.T.)

<sup>\*</sup> Correspondence: chengljia@cdu.edu.cn (L.C.); drshiz1002@hotmail.com (Z.S.)

<sup>†</sup> These authors contributed equally to this work.

**Abstract:** As a biomedical material, porous titanium alloy has gained widespread recognition and application within the field of orthopedics. Its remarkable biocompatibility, bioactivity, and mechanical properties establish it as a promising material for facilitating bone regeneration. A well-designed porous structure can lower the material's modulus while retaining ample strength, rendering it more akin to natural bone tissue. The progression of additive manufacturing (AM) technology has significantly propelled the advancement of porous implants, simplifying the production of such structures. AM allows for the customization of porous implants with various shapes and sizes tailored to individual patients. Additionally, it enables the design of microscopic-scale porous structures to closely mimic natural bone, thus opening up avenues for the development of porous titanium alloy bone implants that can better stimulate bone regeneration. This article reviews the research progress on the structural design and preparation methods of porous titanium alloy bone implants, analyzes the porous structure design parameters that affect the performance of the implant, and discusses the application of porous medical titanium alloys. By comparing the effects of the parameters of different porosity, pore shape, and pore size on implant performance, it was concluded that pore diameters in the range of 500–800  $\mu\text{m}$  and porosity in the range of 70%–90% have better bone-regeneration effects. At the same time, when the pore structure is a diamond, rhombohedral, or cube structure, it has better mechanical properties and bone-regeneration effects, providing a reference range for the application of clinical porous implants.

**Keywords:** 3D printing; titanium alloys; bone implant; porous structure



**Citation:** He, S.; Zhu, J.; Jing, Y.; Long, S.; Tang, L.; Cheng, L.; Shi, Z. Effect of 3D-Printed Porous Titanium Alloy Pore Structure on Bone Regeneration: A Review. *Coatings* **2024**, *14*, 253. <https://doi.org/10.3390/coatings14030253>

Academic Editor: Günter Motz

Received: 22 January 2024

Revised: 12 February 2024

Accepted: 16 February 2024

Published: 20 February 2024



**Copyright:** © 2024 by the authors. Licensee MDPI, Basel, Switzerland. This article is an open access article distributed under the terms and conditions of the Creative Commons Attribution (CC BY) license (<https://creativecommons.org/licenses/by/4.0/>).

## 1. Introduction

The repair and replacement of a wide range of bone defects caused by diseases, trauma, and aging has been an important subject for centuries. So far, the regeneration of bone defects caused by war, infection, car accidents, tumors, and genetics is still a clinical challenge [1]. Bone tissue possesses intrinsic regenerative capabilities, but it has a critical size limit. Within this critical size limit, bone defects can be repaired through the self-healing capacity of the bone tissue itself. However, when bone defects exceed this critical size limit, such as those resulting from trauma, disease, tumor resection, or osteomyelitis, spontaneous healing becomes challenging in the absence of external intervention. A segmental bone defect is defined as a defect whose length exceeds 1.5 times its diameter. At present, the most common treatment methods for bone defects are autologous bone transplantation and allograft bone transplantation. Among them, autologous bone transplantation is considered to be the “gold standard” in clinical practice; that is, it is the most effective bone-regeneration method [2,3]. However, these two treatments have obvious limitations, such as limited autogenous bone, more pain for patients [4], and immune rejection [5]. In view of this, orthopedic alternatives have rapidly developed in response to clinical needs,

including skull prostheses, dental implants, interbody fusion devices, femur prostheses, and tibial prostheses.

Currently, the biomaterials used for implants include the following four categories: metals and their alloys, polymers, ceramics, and natural materials. The properties of several commonly used materials are compared with those of natural human bone, as shown in Table 1. Metal materials exhibit superior mechanical strength and wear resistance in comparison to polymer and ceramic materials, so metal materials are often used as the preferred materials for load-bearing implants [6]. Among all metal materials, titanium alloy (Ti6Al4V) is widely used in the manufacture of orthopedic and dental implants because of its high strength, low density, corrosion resistance, low elastic modulus, and good biocompatibility [7,8]. The elastic modulus of human cortical bone and trabecular bone ranges from 3 GPa to 30 GPa and 0.01 GPa to 3 GPa, respectively [9–11], while the elastic modulus of a traditional solid titanium alloy can reach 110 GPa, which is much higher than the elastic modulus of human bone, so the stress-shielding problem may be faced after implantation [12]. The high contrast between the mechanical properties of bone tissue and implant biomaterials may lead to bone resorption, a phenomenon defined as stress shielding [13], which limits the normal growth of bone and ultimately leads to implantation failure. Secondly, the dense titanium alloy was connected to the host-only interface, and the intensity after implantation was also prone to loosening [14]. To address these issues, titanium alloys with a porous structure have been introduced, and this porous structure is regarded as an effective method for mitigating the mismatch in the elastic modulus [15–17]. Porous titanium alloys combine the advantages of titanium alloys and porous structures and can be used to manufacture implants with a more perfect structure and performance to achieve the effect of reducing the elastic modulus and regulating mechanical properties.

The ideal orthopedic implant requires its structure to conform to the anatomy of natural bone tissue and have connected pores that can satisfy the inward growth and vascularization of cells. It has certain mechanical properties to provide mechanical support and avoid the fatigue fracture of the materials; has a surface suitable for cell adhesion, growth, and reproduction; and should have good biocompatibility and a good bone-tissue-integration ability [18–20]. The design of porous structures involves the porosity, pore size, and shape. The porosity, pore size, and shape of porous scaffolds can play an important role in the growth of cells and the mechanics of the scaffold and will affect cell nutrients, the flow of oxygen, and the biological responses of the cells (such as their proliferation, differentiation, and signaling). The pore structure creates conditions for processes such as cell adhesion, growth, and reproduction [21], allowing for cell migration, the influx of oxygen and nutrients, and the circulation of body fluids [22,23]. Since the introduction of porous Ti6Al4V bone implants, researchers have been diligently striving to discover a porous implant design that is better suited for promoting bone tissue regeneration [4].

**Table 1.** Comparison of properties of various biomaterials.

Material	Yield Strength (MPa)	Strength of Extension (MPa)	Elasticity Modulus (GPa)	Cite
Human bone (Cortical bone)	30–70	70–150	4–30	[24]
CpTi	320	465	110	[25]
Ti6Al4V	585–1060	690–1100	55–110	[26]
Stainless steel	190–690	490–1350	200–210	[27,28]
Co-based alloys	310–1586	655–1793	210–253	[29,30]
Hydroxyapatite	—	40–300	80–120	[31]
Bioglass45S5	—	42	35	[32]

## 2. Preparation of Porous Titanium Alloys

Traditional processing methods such as metal foaming [33], freeze casting [34], and powder metallurgy [35] can be used to manufacture porous structures. However, for im-

plants with complex structures, the traditional methods cannot obtain an accurate porosity, and it is difficult to control their porous structures [36], which limits the application of porous structures in bone implants. In recent years, more and more studies have adopted additive manufacturing technology (also known as 3D printing technology) to manufacture implants with porous structures [37]. Three-dimensional printing technology is a bottom-up processing method. It operates by creating solid objects layer by layer, following computer-generated 3D models. This technology excels in meeting the demands of personalized customization to the fullest extent [38]. Three-dimensional printing technology can further change its elastic modulus and mechanical properties by adjusting parameters such as the pore size, porosity, pore shape, and surface topography. Today, 3D printing technology has been widely used in various fields, including agriculture, healthcare, the automotive industry, and the aerospace industry for mass customization. Figure 1 illustrates the utilization of 3D printing technology across various fields. The advantage of 3D printing in the medical field is that it can be tailored for patients by computer, the size and shape of the defect can be determined by a CT scan, and then the matching 3D model can be built by reverse modeling [39], as shown in Figure 1a. Three-dimensional printing technology can further modify its mechanical and bone-inducing properties through parameter adjustments, such as the pore size, shape, porosity, and surface topography.

Metal additive manufacturing technology can be divided into several different forming processes, including Selective Laser Sintering (SLS), Direct Metal Laser Sintering (DMLS), Selective Hot Sintering (SHS), Selective Laser Melting (SLM), and Electron Beam Selective Melting (SEBM), among others. SLM can make porous titanium structures well, and the Young's modulus of the structure is well matched with that of the skeleton [40]. Therefore, it is often used in the medical field for the molding of porous titanium alloys. Cui et al. [41] prepared porous titanium alloys by using SLM technology. Compared to solid metals, the elastic modulus of porous titanium has been reduced to 0.74 GPa while achieving a compressive yield strength of 201.91 MPa. This meets the requirements for compatibility with human bone tissue, highlighting the advantages of 3D printing technology in fabricating porous structures.

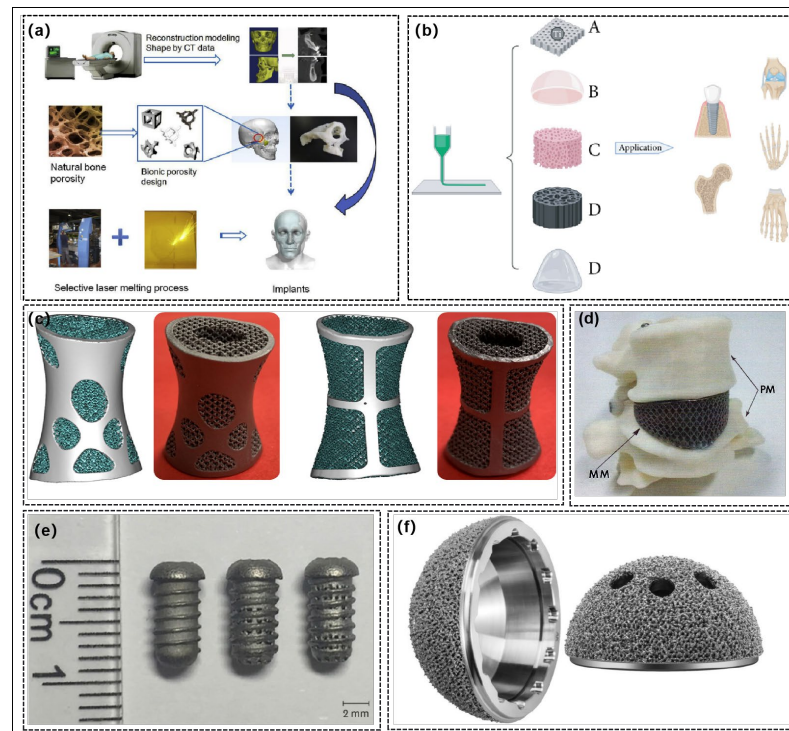


**Figure 1.** (a) Customization process of 3D-printed implants [15]. (b) Application of 3D printing in orthopedics [42]. (c) Three-dimensionally printed artificial vertebral body model and actual pictures [43].

(d) SLM-3D-printed personalized Ti6Al4V spinal cage (mesh) implant [44]. (e) Three-dimensionally printed Ti6Al4V threaded implant specimen [45]. (f) Trabecular titanium acetabular cup produced by 3D ACT EBM [46]. (Reprinted with permission from Ref. [15]. Copyright 2019 Elsevier; Ref. [43]. Copyright 2021 Elsevier. Reprinted from Ref. [42]; Ref. [44]; Ref. [45]; Ref. [46]).

### 3. Effect of 3D Printing Porous Titanium Alloy Pore Structure on Bone Regeneration

Although a large number of porous metal implants have been designed, the design and properties of porous structures are still subject to extensive research, especially the effects of porosity, pore size, and shape. At present, there is no unified conclusion on the optimal values of the pore size, porosity, and other parameters. In order to find suitable porous structures, the effects of the above three structures on the physical properties and endogenous bone growth of titanium implantation are discussed below. In order to find suitable porous structures, the effects of the above three structures on the physical properties and endogenous bone growth of titanium implantation are discussed below.

#### 3.1. Porosity

Porosity is the ratio of the porous portion to the solid portion of the scaffold. Porosity characteristics are usually obtained indirectly through physical measurements (for example, using the density principle, immersing the sample in water, placing it in a graduated cylinder, replacing the volume of water with the actual volume of the scaffold, and obtaining porosity data based on the difference in volume) or by using digital image processing and analysis, as well as computed tomography techniques that can provide a more direct way to obtain porosity data [47]. The porosity is calculated as follows:

$$\eta = \frac{V_p}{V_z} \times 100 \%$$

Here,  $V_p$  represents the pore volume of the scaffold, while  $V_z$  denotes the original volume of the scaffold.

The elastic modulus of implants is mainly regulated by porosity and can be changed by adjusting the porosity. At the same time, porosity plays an important role in establishing early bone integration and forming strong interface bonding between porous implants and surrounding tissues [48]. Increasing porosity provides more room for cells to grow, and the transport of oxygen and nutrients is correspondingly increased [49]. However, adding too high a porosity with the same structural design can lead to a significant decrease in mechanical properties, so finding the optimal porosity range is crucial for the successful application of the implant. The right porosity can provide cells with room to reproduce while mimicking the pore structure and mechanical strength of natural bone tissue [15]. When the porosity of the implant matches that of the human bone, the optimal bone growth environment can be obtained. The structural variations in porous scaffolds with different porosities are illustrated in Figure 2. Natural bone tissue comprises two distinct structures: cancellous bone and cortical bone. The interior of cancellous bone features a spongy structure with a porosity ranging from 50% to 90%. The internal structure of cortical bone is dense, the bone density is much lower than that of cancellous bone, and the porosity is only 5% to 10%. Scaffolds with a porosity comparable to that of human bone trabeculae (70% to 90%) have been shown to enhance cell viability and inward bone growth [50,51]. Moreover, studies have shown that when the porosity is greater than 70%, the porosity of the porous structure can have a beneficial effect on bone tissue [52]. A scaffold structure with a 600–900  $\mu\text{m}$  pore size and 60%–90% porosity is recommended as the best structure [53]. Zhang et al. [54] differentiated the pore rate of a 3D-printed preparation (40%, 70%, and 90%), and the pore diameter was 700  $\mu\text{m}$  multipores. Micro-CT results showed that the bone integration effect of the implant with a porosity of 40% (P40) was inferior to that of the implant with a porosity of 70% (P70) and 90% (P90). In addition, it is suggested that the change in pore size has a more significant effect on osteogenesis when the porosity is in the range of 70%–90%. In recent years, more and more researchers

have prepared porous titanium alloys with a gradient structure. Hindy et al. [40] follow the biomimetic approach and apply the porosity gradient visible in natural bone to the fabrication of orthopedic and dental implants. The replication of this functional gradient ensures the correct distribution of the compression stiffness in different regions.

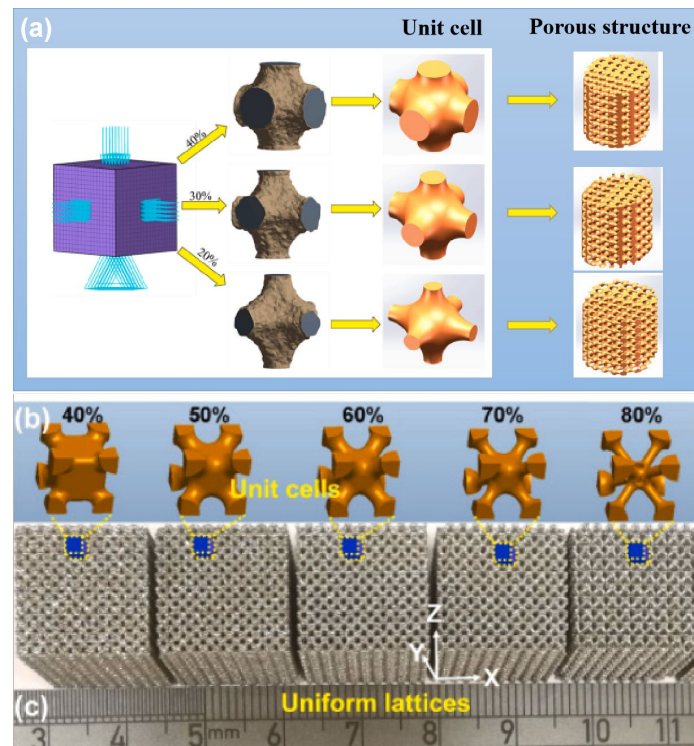


**Figure 2.** (a) Structural change model of porous scaffolds with different porosity [55]. (b) Unit cells with different structural porosity [56]. (c) The LPBF-processed uniform lattice samples [56]. (Reprinted with permission from Ref. [55]. Copyright 2023 Elsevier; Ref. [56]. Copyright 2021 Elsevier).

### 3.2. Pore Configuration

Most studies only explored the porosity and pore size suitable for endogenous bone growth under the condition of a fixed pore shape and ignored the fact that the pore shape of a porous structure would also affect the effective spatial distribution of the cells inside the scaffold and affect the mechanical properties of the scaffold. The pore shape was originally designed to mimic the shape of micropores inside the natural human bone, which is a complex tissue with a precise porous structure. There are different opinions about the micropore structure of bone tissue. Some people think that the microholes inside the human bones are round, some people observe that they are square holes, and some people think that they are hexagonal honeycomb holes. The geometry of the holes in bone implants can be square, rectangular, spherical, trabecular, or hexagonal, and more complex shapes can be made by using solid free-form fabrication techniques, such as cubes [57], diamonds [58], rhombohedrons [41], and variations of these structures. With different pore shapes, the mechanical properties and osteogenic properties of the scaffolds are also different. For instance, the diamond structure has two additional angles compared to the cubic structure, thereby offering a larger adhesive surface area for cells. The internal topologies of the porous materials designed by computer-aided methods can be roughly divided into (1) spatially arranged units composed of pillars, (2) three-period minimum surfaces (TPMSs), and (3) irregular bioinspired or Voronoi Mosaic structures. In recent years, TPMSs have also been widely applied to the field of bone tissue engineering based on naturally occurring nanoscale spiral structures found on butterfly wings that have an average curvature value of zero while the average curvature value of human trabecular

bones is also close to zero [17]. A TPMS is an infinite and periodic surface, and the TPMS is often described by the following types of equations:

$$\cos \alpha x + \cos \beta y + \cos \gamma z = c$$

This equation satisfies the equation  $\varphi(x, y, z) = c$ , and this function  $\varphi(x, y, z)$  is the isosurface evaluated by the isosurface  $c$ .

TPMS structures, including gyro, primitive, and diamond structures, are generated by using mathematical formulas to tune their mechanical properties by changing various parameters such as the periodicity and relative density. Kelly et al. [17] evaluated the performance of TPMS titanium scaffolds produced by AM to repair femoral defects in rats and confirmed that TPMS scaffolds can repair segmental bone defects. Table 2 summarizes studies of the biological properties of AM implants with different structures. Jahir-Hussain et al. [59] conducted a comparative analysis of the mechanical properties of 3D-printed polylactide (PLA) scaffolds with four distinct pore structures, including round, square, hexagonal, and triangular, by utilizing finite element analysis (FEA). Their findings revealed that scaffolds featuring hexagonal pore shapes exhibited mechanical properties consistent with those of human bones. Van Bael et al. [60] discovered that, in comparison to hexagonal holes, triangular holes were more favorable for cell growth and differentiation, whereas rectangular holes were more prone to causing cell blockage. By examining local curvature and pore shapes, it was determined that obtuse angles were more likely to result in cell blockage compared to acute angles. However, Xu et al. [61] reported that the osteogenic ability of hexagonal prism scaffolds was higher than that of triangular prism scaffolds through in vivo and in vitro studies. Zhao et al. [62] reported the influence of tetrahedral and octahedral cell scaffolds on cell affinity and found that octahedral cells exhibit better static mechanical properties and a longer fatigue life than tetrahedral cells. At the same time, cells spread better on the scaffold on the octahedron than on the tetrahedron.

Kovács et al. [63] studied the mechanical properties and bone inward growth effect of titanium alloy scaffolds with six lattice shapes, including a gyro type, cube, cylinder, tetrahedron, diagonal cone, and Tyson polygon. The efficiency of the bone inward growth of several lattice shapes was compared, and the results showed that the bone growth degree of the gyro, conical, and cubic lattices was the best. Lim et al. [64] also came to the same conclusion by implanting titanium scaffolds of three different structures (octadense, gyroid, and dode) into the femur of rabbits, and no differences in bone formation in the titanium scaffolds were observed between the three types of pore structures. Farazin et al. [65] compared the biocompatibility of the cube, pyramid, and diagonal pore structures and found that the pyramid structures had the highest cell viability and migration ability. Deng et al. [66] conducted a study to investigate the effect of 3D-printed scaffolds with four different pore structures (i.e., diamond, tetrahedral cells, round pores, and cubes) on the osteogenic properties. The results showed that the diamond structure produced the best bone growth, possibly because the structure's strut angles are similar to the angles between the trabeculae of cancellous bone in humans. At the same time, fluid dynamics (CFD) studies also show that the diamond structure has the smallest fluid velocity difference and the longest fluid flow path. This property is very beneficial for promoting blood vessel development, promoting nutrient transport, and enhancing bone formation. Therefore, the diamond structure is more conducive to bone growth. Compared with diamond structures, rhombohedral dodecahedrons have been shown to have better mechanical strength and moderate biological properties and can be applied to body parts with relatively high mechanical properties requirements [67]. Zhao et al. [15] conducted a study on the mechanical properties of supports featuring various pore structure elements. The findings revealed that supports with diamond-shaped pore elements exhibited the lowest compressive strength, measuring only approximately 38.2 MPa. Supports featuring cyclopore elements displayed a lower compressive strength, around 57.0 MPa, while those with cube-shaped pore elements demonstrated a higher compressive strength, approximately 142.8 MPa. In summary, the diamond structure, rhombohedral dodecahedron structure, and cube structure show great potential in promoting bone regeneration.

**Table 2.** Common porous scaffold structures and their characteristics.

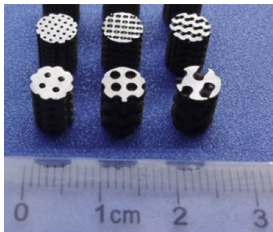
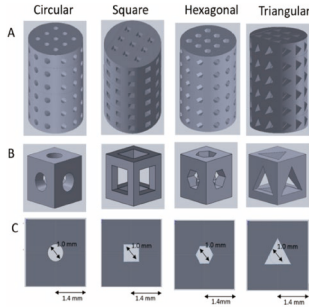
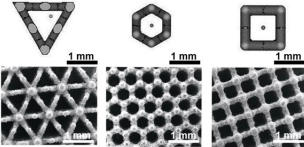
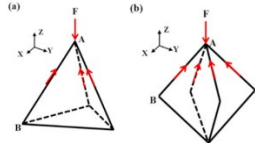
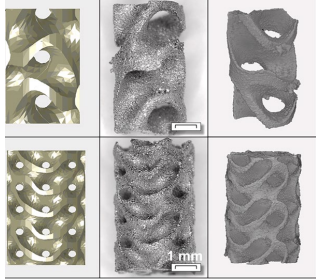
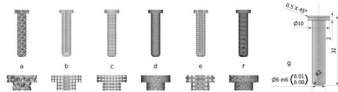
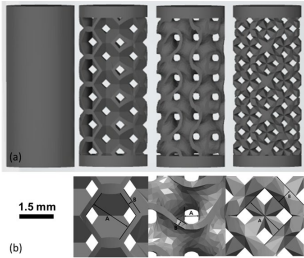
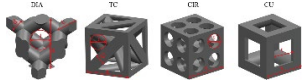
Pore Size ( $\mu\text{m}$ )	Porosity (%)	Pore Structure	Cell Structure	Conclusions	Ref.
500	80 75 70 65 60	Diamond Gyroid Orthogonal Cube Truss		Truss and cube structures have higher compressive strength. Diamond and gyroid structures have lower compressive strength, which may be due to the complex porosity and small vertical solid-bearing surface of these two structures.	[15]
100	—	Circular Square Hexagonal Triangular		The results of the finite element analysis (FEA) indicate that scaffolds with a hexagonal pore shape exhibit greater similarity in performance to human bones.	[59]
500	—	Triangle Hexagon Rectangle		Rectangular pore is easy to cause cell blockage. Compared with hexagonal, triangular pore structure is more conducive to cell growth and differentiation.	[60]
500 1000	67 62.87 84 77	Tetrahedron Octahedron	 F represents compressive stress, and the red arrow represents tensile stress.	The adhesion of scaffolds with 1000 apertures was superior, but their compressive and fatigue properties were inferior to those of scaffolds with 500 apertures. Octahedral scaffolds exhibited better compression performance and fatigue life compared to tetrahedral scaffolds, and they also displayed a greater capacity for cell proliferation.	[62]

Table 2. Cont.

Pore Size (μm)	Porosity (%)	Pore Structure	Cell Structure	Conclusions	Ref.
1076 739	70	Gyroid		Titanium gyroid-sheet scaffolds can be used to repair segmental defects, and small-hole gyroscaffolds exhibit considerable inward-facing growth compared to large-hole gyroscaffolds. There was no significant difference in torsional strength and stiffness of the small pore implant compared with intact femur.	[17]
600	—	Gyroscope Cube cylinder tetrahedron Double pyramid Voronoi		Six lattice shapes, gyroscope, cube, cylinder, tetrahedron, double pyramid, and Voronoi, were ranked for bone growth efficiency, and gyro, double pyramid, and cube lattice implants had the highest bone tissue growth per unit time.	[63]
1070 300 760	75	Octedens Gyroid Dode	 <p>A: pore size, B: strut thickness.</p>	No differences in bone formation in titanium scaffolds were observed between the three types of pore structures.	[64]
650	65	Diamond Tetrahedro Cell Circular Cube		Diamond structure has the best bone growth, and fluid dynamic analysis also shows that this structure is conducive to blood vessel growth and bone formation.	[66]

### 3.3. Pore Size

The porous structure not only efficiently lowers the elastic modulus, encouraging the formation of a mineralized layer on the implant's surface and promoting protein adsorption, but also offers a conducive environment for cell adhesion, thereby facilitating the proliferation and differentiation of bone cells. Additionally, it serves as a channel for the transmission of metabolism and nutrition [68]. The pore size is very important for porous implants, and it affects the expression of osteogenic genes and the differentiation of osteoblasts. Wang et al. [69] confirmed that pore size and structure also play a certain role in regulating the expression of genes related to angiogenesis. The aperture of the scaffold should ensure that bone cells, nerve fibers, and blood vessels can grow into the scaffold. When the aperture is too large, it increases air permeability, which prevents cells from adhering to the surface [70]. When the aperture is too small, cells cannot enter the scaffold, resulting in cell accumulation, reducing cell migration in the scaffold and even affecting the circulation of nutrients and metabolic waste, which is not conducive to the growth of bone tissue [52]. At present, there is no precise definition of the most suitable pore size for bone growth. Some studies generally believe that the pore size of 100  $\mu\text{m}$  to 400  $\mu\text{m}$  can promote angiogenesis and bone growth, and below this range will limit bone cell growth [71]. Through a comprehensive analysis of the pore size required for the internal growth space of bone tissue and the formation of blood vessels, it is recommended that the optimal pore size is 300–600  $\mu\text{m}$  [72,73]. The comprehensive impact of pore size on implants is summarized and drawn Figure 3. After staining with Toluidine Blue, it was observed that new bone tissue had developed within nearly all of the surface micropores of the 600  $\mu\text{m}$  implants. The results indicate that, in comparison to scaffolds with 200  $\mu\text{m}$  and 1000  $\mu\text{m}$  apertures, the scaffolds featuring 600  $\mu\text{m}$  apertures were more favorable for the growth of new bone tissue. Zhao et al. [62] reported tetrahedral cell titanium alloy scaffolds with pore sizes of 500  $\mu\text{m}$  and 1000  $\mu\text{m}$ . Figure 4a shows that cells on the scaffold with a pore size of 1000  $\mu\text{m}$  exhibit better spread and more filamentous pseudopods. Hara et al. [74] conducted an experiment in which they implanted four types of cylindrical porous titanium alloys with varying pore sizes (500  $\mu\text{m}$ , 640  $\mu\text{m}$ , 800  $\mu\text{m}$ , and 1000  $\mu\text{m}$ ) into the distal end of rabbit femurs. The findings revealed that porous titanium alloys with pore sizes smaller than 800  $\mu\text{m}$  offered bioactive surfaces and maintained mechanical stability for bone fixation through implants. Meanwhile, Zhou et al. [75] proposed that the pore size of ideal bone tissue engineering scaffolds should be 300–900  $\mu\text{m}$ . Zhang et al. [54] prepared titanium alloy scaffolds with a constant porosity of 70% and different pore sizes (400  $\mu\text{m}$ , 700  $\mu\text{m}$ , and 900  $\mu\text{m}$ ) and porous titanium alloy scaffolds with constant pore sizes of 700  $\mu\text{m}$  and different porosities (40%, 70%, and 90%). The effect of the pore size and porosity on osteogenesis was discussed. The micro-CT results showed that a scaffold with a pore size of 700  $\mu\text{m}$  can better induce cell ingrowth and new bone formation. An interesting phenomenon was discovered through fluorescence images; that is, cells are more likely to grow at the edges and then spread toward the center. Within the recommended porosity range (70%–90%), changes in pore size have a more significant impact on osteogenesis. Similarly, the same phenomenon was found in a study by Ran et al. [76]. The actual pore sizes of P500/P700/P900 implants prepared by SLM were  $401 \pm 26 \mu\text{m}$ ,  $607 \pm 24 \mu\text{m}$ , and  $801 \pm 33 \mu\text{m}$ , respectively. Through observation, the morphology of osteoblasts on different implants found that the larger the pore size, the higher the cell density, as shown in Figure 4b,c. Finally, by implanting the implant into rabbits, it was concluded that the biological performance of the P700 group with an actual pore diameter of approximately 600  $\mu\text{m}$  was better than that of the other two groups. Wang et al. [77] created consistently sized cubic pores measuring 300  $\mu\text{m}$ , 400  $\mu\text{m}$ , 500  $\mu\text{m}$ , 600  $\mu\text{m}$ , 700  $\mu\text{m}$ , 800  $\mu\text{m}$ , 900  $\mu\text{m}$ , and 1000  $\mu\text{m}$  through a combination of in vivo and in vitro experiments. The structural modifications and experimental outcomes are depicted in Figure 4d–f. The cell adhesion, proliferation, and differentiation of the 500  $\mu\text{m}$ , 600  $\mu\text{m}$ , and 700  $\mu\text{m}$  porous scaffolds were superior to those of the other groups. Subsequent in vivo experiments showed that the 600  $\mu\text{m}$  porous scaffolds had a better ability to induce new bone formation. Ouyang [78] compared the correlation between

the mechanical properties and bone regeneration of scaffolds with a 400  $\mu\text{m}$ , 650  $\mu\text{m}$ , 850  $\mu\text{m}$ , and 1100  $\mu\text{m}$  aperture prepared by SLM and finally showed that the scaffolds with a 650  $\mu\text{m}$  aperture showed the best bone inward growth.

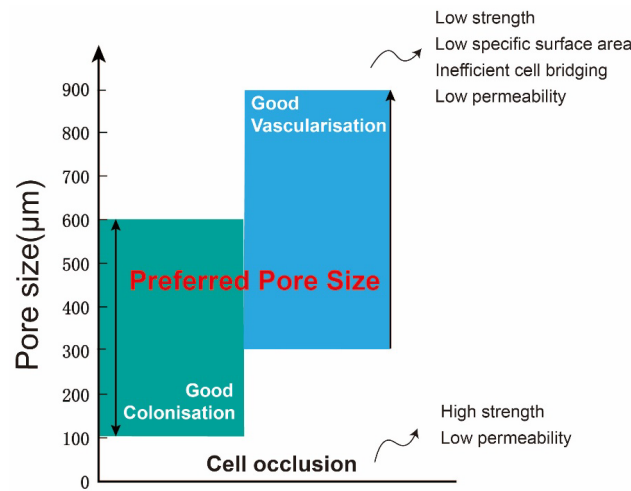


Figure 3. Comprehensive effect of pore size on implants.

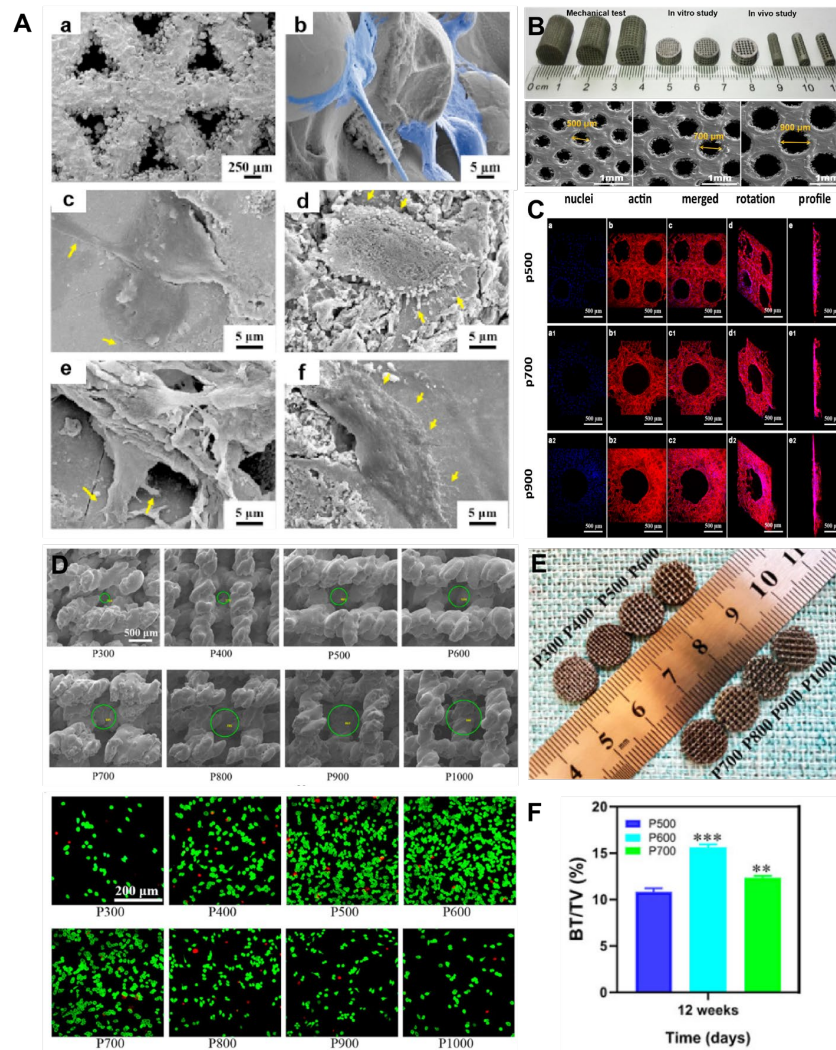


Figure 4. Effect of porous titanium scaffolds with different pore size and porosity on osteogenesis and cells. (A): SEM micrographs of cells after 3 days of culture with scaffolds: a on the surface, b into

pores. Pseudopodia are in blue. SEM morphology of cells after 3 days of culture on c T500, d T1000, e O500, f O1000. Lamellipodia and filopodia are indicated by yellow arrows in c–f [62]. (B): Macrophotographs of 3D-printed porous Ti6Al4V samples used for mechanical testing and in vitro and in vivo studies, and SEM images of p500, p700, and p900 [76]. (C): Representative fluorescence images of osteoblast adhesion to porous Ti6Al4V implants after 14 days of culture. Cells are stained with actin filaments (red) and nuclei (blue) [76]. (D): Pore size analysis of Ti6Al4V and cell-staining results (live: green; dead: red), the green circle represents the pore size measured by Image-J software (Version 1.54) [77]. (E): Optical pictures of porous titanium alloys with different pore sizes [77]. (F): Quantitative analysis of BV/TV [77] ( $p < 0.05$ ,  $** p < 0.01$ , and  $*** p < 0.001$ , when compared with P500). (Reprinted with permission from Ref. [62]. Copyright 2023 Elsevier. Reprinted from Ref. [76]; Ref. [77]).

#### 4. Application of 3D-Printed Titanium Alloy Bone-Repair Scaffolds

The utilization of 3D-printed porous titanium alloys addresses the issue of a mismatched elastic modulus between implants and human bone, enhancing compatibility with host bone tissue. Consequently, this technology finds frequent application in orthopedic bone defect repair and dental implant procedures. This section is dedicated to discussing the use of titanium-alloy-based orthopedic and dental implants. A single porous titanium alloy alone may not suffice to address the common challenges encountered in clinical practice. In practical research and application, it is often combined with other functional materials to achieve enhanced performance and functionality [62].

Biomimetic modifications can optimize the biocompatibility of the surface of 3D-printed porous structures, imparting various desirable properties. The judicious selection of biomaterial coatings represents a straightforward and effective approach to augment the biological activity of 3D-printed implants. For example, Wei et al. [79] used 3D printing technology to prepare a porous titanium alloy scaffold with a porosity of 68% and a pore size of 710  $\mu\text{m}$  and then used multiarc ion plating technology to prepare a magnesium coating on the scaffold. Magnesium and its alloy also have good biocompatibility, and the most important thing is that it is a degradable material. The results showed that magnesium ions would be released after implantation, and the appropriate concentration of magnesium ions could inhibit the proliferation of bone tumor cells. Porous titanium is combined with antibacterial hydrogel to fill the micropores of porous titanium, which can be used to treat infected bone defects to induce bone repair and bone integration. Qiao et al. [80] 3D printed a titanium scaffold with a porosity of 70% and a pore size of 600  $\mu\text{m}$  and found that the regenerated bone tissue around the bare titanium scaffold was very limited while the composite implant showed an antibacterial ability and the ability to promote the bone formation differentiation of bone marrow mesenchymal stem cells (BMSCs) in both in vivo and in vitro experiments. More applications are shown in Table 3.

Table 3. Application case of porous titanium alloy implants.

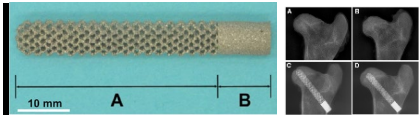
Material	Method	Feature	Outcome	Ref.
Ti-6Al-4V	EBM	 <p>3D printed porous titanium is a porous titanium alloy rod with a diamond lattice prepared using electron beam melting (EBM) technology. A: the body of the rod; B: the end of the rod.</p>	Following Ti-Rod implantation, the femoral head showed good osseointegration, with tight integration between the peripheral bone and the rod, and the new bone grew along the metal trabecula without the intervention of fibrous tissue.	[81]

Table 3. Cont.

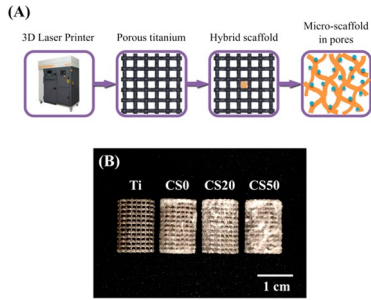
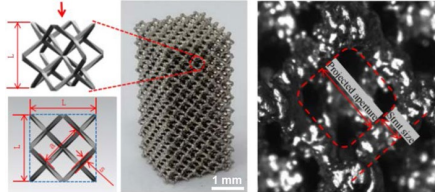
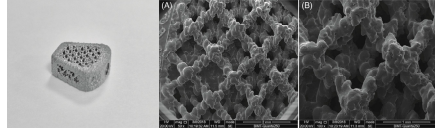
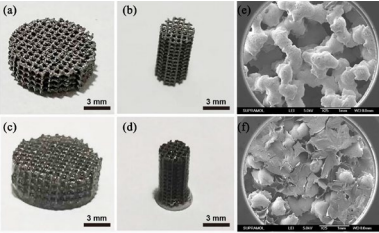
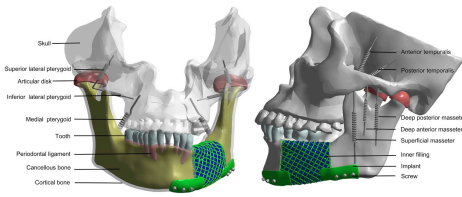
Material	Method	Feature	Outcome	Ref.
Ti-6Al-4V	SLM	 <p>The aperture of the 3D-printed Ti-6Al-4V stent is about 350 <math>\mu\text{m}</math>, and the maximum compressive strength is <math>49.3 \pm 0.9</math> MPa. (A) is the preparation and coating scheme of 3D printed Ti6Al4V scaffold. (B) is a photographic image of Mg-CS/CH coated Ti6-Al-4V scaffold.</p>	The Mg-CS/CH-coated Ti-6Al-4V scaffold enhanced cell adhesion, proliferation, and differentiation, thereby enhancing downstream osteogenesis and mineralization.	[6]
Ti-6Al-4V	EBM	 <p>Titanium alloy cells (<math>L</math>, <math>a</math> and <math>s</math> are unit, projected aperture and strut size, respectively) were designed to simulate trabecular structure.</p>	Compared to the solid titanium alloy structure, the elastic modulus of the 3D-printed titanium alloy scaffold with a trabecular structure ranges from 0.39 to 0.618 GPa, which closely approximates that of natural bone. This characteristic helps mitigate the occurrence of stress-shielding phenomena.	[82]
Ti-6Al-4V	EBM	 <p>(a) SEM image of the new 3D cage at 50 times; (b) SEM image of the new 3D cage at 100 times. The interior of the 3D-printed cage has an octahedral porous structure with uniform pore size and interconnectivity.</p>	New bone grows inside the cage through pores on the surface of the newly 3D-printed cage. This 3D-printed porous titanium cage exhibits excellent biocompatibility and osseointegration capabilities, making it a potential candidate for clinical applications.	[83]
Ti-6Al-4V	EBM	 <p>Visual images of (a) disk-shaped and (b) columnar-shaped pTi scaffolds. Visual images of supramolecular hydrogel modified (c) disk-shaped and (d) columnar-shaped pTi scaffolds. SEM microphotographs of (e) pTi scaffolds and (f) supramolecular hydrogel modified pTi scaffolds.</p>	Hydrogels composed of sodium tetraborate, polyvinyl alcohol, silver nanoparticles, and tetraethyl orthosilicate were combined with titanium alloy scaffolds for the treatment of infected bone defects. In vivo experiments verified that these implants can promote bone regeneration while effectively exhibiting antibacterial properties.	[80]

Table 3. Cont.

Material	Method	Feature	Outcome	Ref.
Ti-6Al-4V	—	 <p>A 3D-printed titanium mesh used to repair mandibular defects.</p>	Through finite element analysis, the optimized implant can provide an excellent mechanical environment for bone regeneration, so as to achieve long-term stability and occlusion reconstruction of the implant.	[84]

## 5. Conclusions

The 3D-printed porous titanium alloy bone-repair scaffold can effectively solve the stress-shielding problem between the implant and human bone, solve the bone mismatch problem, shorten the operation time, and reduce the surgical failure rate, and it is expected to solve the clinical problem of large bone defects repair, which has been widely studied and applied in recent years. In this study, we conducted a comprehensive review of the influence of structural design in 3D-printed orthopedic titanium alloy implants on bone regeneration. We examined the critical factors such as pore size, porosity, and pore shape that can effectively enhance bone regeneration. This analysis offers valuable insights and establishes a reference framework for future research endeavors focused on the structural aspects of porous implants. Based on the discussion of the above literature, the pore size range of 500–800  $\mu\text{m}$  and the porosity range of 60%–90% can achieve a better bone growth effect. The cell structures with a better bone regeneration effect were diamond, rhombohedral dodecahedron, and cube.

## 6. Future Direction

While 3D printing porous titanium alloy offers numerous advantages, it still encounters certain practical challenges. There is a need for further refinement in both the design of porous structures and the selection of titanium alloy materials for 3D printing porous titanium alloy brackets. First of all, the porous structure of a human skeleton is not uniformly distributed on the whole but presents a gradient porous structure with a dense exterior and loose interior. In the future, bionic porous scaffolds that can balance biological and mechanical properties should be further studied to achieve the perfect combination of implants and human bones. Secondly, efforts should be made to research the composition of titanium alloys to improve the performance of titanium alloys, thereby preparing stents with better performance. Finally, in order to verify the long-term safety and effectiveness of porous titanium alloys, more clinical experiments and research are needed to combine porous titanium implants with other functional materials to achieve antibacterial, osteogenic, and other effects and obtain more clinical data and experience. With the deepening of research, 3D printing will be able to exert greater value in combination with artificial intelligence and big data in the future.

**Author Contributions:** Writing—original draft preparation, S.H. and L.C.; writing—review and editing, J.Z. and Z.S.; formal analysis, Y.J. and S.L.; data curation, L.T. All authors have read and agreed to the published version of the manuscript.

**Funding:** This work was supported by the Natural Science Foundation of Sichuan Province, China (2022NSFSC1510), the Medical Scientific Research Project of Chengdu City, China (2021043), the Sichuan Provincial Science and Technology Foundation (22NZZH0031), and the higher education talent training quality and teaching reform project of the education department of Sichuan Province, China (JG2021-1102).

**Institutional Review Board Statement:** Not applicable.

**Informed Consent Statement:** Not applicable.

**Data Availability Statement:** Data are contained within the article.

**Conflicts of Interest:** The authors declare no conflicts of interest.

## References

1. Ruales-Carrera, E.; Engler, M.L.P.D.; Vaz, P.; Özcan, M.; Volpato, C.A.M. Esthetic and functional rehabilitation of bilateral congenital absence of maxillary lateral incisors: Minimally invasive surgical and prosthetic approach. *J. Esthet. Restor. Dent.* **2019**, *31*, 5–12. [[CrossRef](#)]
2. García-Gareta, E.; Coathup, M.J.; Blunn, G.W. Osteoinduction of bone grafting materials for bone repair and regeneration. *Bone* **2015**, *81*, 112–121. [[CrossRef](#)]
3. Sun, Q.; Li, Z.; Liu, B.; Yuan, X.; Guo, S.; Helms, J.A. Improving intraoperative storage conditions for autologous bone grafts: An experimental investigation in mice. *J. Tissue Eng. Regen. Med.* **2019**, *13*, 2169–2180. [[CrossRef](#)]
4. Li, J.; Zhong, H.; Cao, B.; Ran, Z.; Tan, J.; Deng, L.; Hao, Y.; Yan, J. Comparative Study of 3D-Printed Porous Titanium Alloy with Rod Designs of Three Different Geometric Structures for Orthopaedic Implantation. *Acta Metall. Sin. Engl.* **2023**, *37*, 54–66. [[CrossRef](#)]
5. Donkiewicz, P.; Benz, K.; Kloss-Brandstätter, A.; Jackowski, J. Survival rates of dental implants in autogenous and allogeneic bone blocks: A systematic review. *Medicina* **2021**, *57*, 1388. [[CrossRef](#)]
6. Tsai, C.H.; Hung, C.H.; Kuo, C.N.; Chen, C.Y.; Peng, Y.N.; Shie, M.Y. Improved bioactivity of 3D printed porous titanium alloy scaffold with chitosan/magnesium-calcium silicate composite for orthopaedic applications. *Materials* **2019**, *12*, 203. [[CrossRef](#)] [[PubMed](#)]
7. Zhang, B.; Pei, X.; Zhou, C.; Fan, Y.; Jiang, Q.; Ronca, A.; D’Amora, U.; Chen, Y.; Li, H.; Sun, Y. The biomimetic design and 3D printing of customized mechanical properties porous Ti6Al4V scaffold for load-bearing bone reconstruction. *Mater. Des.* **2018**, *152*, 30–39. [[CrossRef](#)]
8. Chowdhury, S.; Arunachalam, N. Surface functionalization of additively manufactured titanium alloy for orthopaedic implant applications. *J. Manuf. Process.* **2023**, *102*, 387–405. [[CrossRef](#)]
9. Lu, X.; Zhang, D.; Xu, W.; Yu, A.; Zhang, J.; Tamaddon, M.; Zhang, J.; Qu, X.; Liu, C.; Su, B. The effect of Cu content on corrosion, wear and tribocorrosion resistance of Ti-Mo-Cu alloy for load-bearing bone implants. *Corros. Sci.* **2020**, *177*, 109007. [[CrossRef](#)]
10. Gautam, D.; Rao, V.K. Nondestructive evaluation of mechanical properties of femur bone. *J. Nondestruct. Eval.* **2021**, *40*, 22. [[CrossRef](#)]
11. Katz, J.L. Anisotropy of Young’s modulus of bone. *Nature* **1980**, *283*, 106–107. [[CrossRef](#)]
12. Zhang, Y.; Sun, B.; Zhao, L.; Yang, G. Design and manufacturing of a novel trabecular tibial implant. *Materials* **2023**, *16*, 4720. [[CrossRef](#)]
13. Raffa, M.L.; Nguyen, V.H.; Hernigou, P.; Flouzat-Lachaniette, C.H.; Haiat, G. Stress shielding at the bone-implant interface: Influence of surface roughness and of the bone-implant contact ratio. *J. Orthop. Res.* **2021**, *39*, 1174–1183. [[CrossRef](#)]
14. Wang, S.; Liu, L.; Li, K.; Zhu, L.; Chen, J.; Hao, Y. Pore functionally graded Ti6Al4V scaffolds for bone tissue engineering application. *Mater. Des.* **2019**, *168*, 107643. [[CrossRef](#)]
15. Zhao, L.; Pei, X.; Jiang, L.; Hu, C.; Sun, J.; Xing, F.; Zhou, C.; Fan, Y.; Zhang, X. Bionic design and 3D printing of porous titanium alloy scaffolds for bone tissue repair. *Compos. B Eng.* **2019**, *162*, 154–161. [[CrossRef](#)]
16. Zhang, L.C.; Liu, Y.; Li, S.; Hao, Y. Additive manufacturing of titanium alloys by electron beam melting: A review. *Adv. Eng. Mater.* **2018**, *20*, 1700842. [[CrossRef](#)]
17. Kelly, C.N.; Lin, A.S.; Leguineche, K.E.; Shekhar, S.; Gall, K. Functional repair of critically sized femoral defects treated with bioinspired titanium gyroid-sheet scaffolds. *J. Mech. Behav. Biomed. Mater.* **2021**, *116*, 104380. [[CrossRef](#)]
18. Vetric, M.; Parizek, M.; Hadraba, D.; Kukackova, O.; Brus, J.; Hlidkova, H.; Komankova, L.; Hodan, J.; Sedlacek, O.; Slouf, M. Porous heat-treated polyacrylonitrile scaffolds for bone tissue engineering. *ACS Appl. Mater. Interfaces* **2018**, *10*, 8496–8506. [[CrossRef](#)]
19. Yao, Q.; Liu, Y.; Selvaratnam, B.; Koodali, R.T.; Sun, H. Mesoporous silicate nanoparticles/3D nanofibrous scaffold-mediated dual-drug delivery for bone tissue engineering. *J. Control Release* **2018**, *279*, 69–78. [[CrossRef](#)]
20. Sharma, A.; Molla, M.S.; Katti, K.S.; Katti, D.R. Multiscale models of degradation and healing of bone tissue engineering nanocomposite scaffolds. *J. Nanomech. Micromech.* **2017**, *7*, 04017015. [[CrossRef](#)]
21. Liu, C.; Wang, C.-y.; Liu, H.; Wang, Z.-h.; Lin, G.-y. Mechanical properties and biocompatibility of 3D printing Ti6Al4V titanium alloy scaffolds. *Zhongguo Youse Jinshu Xue Chin. J. Nonferrous Met.* **2018**, *28*, 758–765.
22. Oladapo, B.I.; Zahedi, S.A.; Ismail, S.O. Mechanical performances of hip implant design and fabrication with PEEK composite. *Polymer* **2021**, *227*, 123865. [[CrossRef](#)]
23. Xu, C.; Zhang, H.; Yu, S.; Wu, W.; Zhang, L.; Liu, Q.; Ren, L. Direct ink writing of porous Fe scaffolds for bone implants: Pore size evolution and effect on degradation and mechanical properties. *J. Mater. Res. Technol.* **2023**, *25*, 4901–4912. [[CrossRef](#)]
24. Nguyen, L.H.; Annabi, N.; Nikkhah, M.; Bae, H.; Binan, L.; Park, S.; Kang, Y.; Yang, Y.; Khademhosseini, A. Vascularized bone tissue engineering: Approaches for potential improvement. *Tissue Eng. Part B Rev.* **2012**, *18*, 363–382. [[CrossRef](#)]
25. Hacisalihoglu, I.; Samancioglu, A.; Yildiz, F.; Purcek, G.; Alsaran, A. Tribocorrosion properties of different type titanium alloys in simulated body fluid. *Wear* **2015**, *332*, 679–686. [[CrossRef](#)]

26. Yu, G.; Li, Z.; Li, S.; Zhang, Q.; Hua, Y.; Liu, H.; Zhao, X.; Dhaidhai, D.T.; Li, W.; Wang, X. The select of internal architecture for porous Ti alloy scaffold: A compromise between mechanical properties and permeability. *Mater. Des.* **2020**, *192*, 108754. [[CrossRef](#)]
27. Gerlich, D.; Hart, S. Pressure dependence of the elastic moduli of three austenitic stainless steels. *J. Appl. Phys.* **1984**, *55*, 880–884. [[CrossRef](#)]
28. Heary, R.F.; Naresh, P.; Sujitha, S.; Nitin, A. Elastic modulus in the selection of interbody implants. *J. Spine Surg.* **2017**, *3*, 163. [[CrossRef](#)]
29. Davis, J.R. *Handbook of Materials for Medical Devices*; ASM International: Materials Park, OH, USA, 2003.
30. Park, J.; Lakes, R.S. *Biomaterials: An Introduction*; Springer: Berlin/Heidelberg, Germany, 2007.
31. Osuchukwu, O.A.; Salihi, A.; Abdullahi, I.; Abdulkareem, B.; Nwannenna, C.S. Synthesis techniques, characterization and mechanical properties of natural derived hydroxyapatite scaffolds for bone implants: A review. *SN Appl. Sci.* **2021**, *3*, 1–23. [[CrossRef](#)]
32. Aufa, A.; Hassan, M.Z.; Ismail, Z. Recent advances in Ti-6Al-4V additively manufactured by selective laser melting for biomedical implants: Prospect development. *J. Alloys Compd.* **2022**, *896*, 163072. [[CrossRef](#)]
33. Parthasarathy, J.; Starly, B.; Raman, S.; Christensen, A. Mechanical evaluation of porous titanium (Ti6Al4V) structures with electron beam melting (EBM). *J. Mech. Behav. Biomed. Mater.* **2010**, *3*, 249–259. [[CrossRef](#)] [[PubMed](#)]
34. Yook, S.W.; Kim, H.E.; Koh, Y.H. Fabrication of porous titanium scaffolds with high compressive strength using camphene-based freeze casting. *Mater. Lett.* **2009**, *63*, 1502–1504. [[CrossRef](#)]
35. Oh, I.-H.; Nomura, N.; Masahashi, N.; Hanada, S. Mechanical properties of porous titanium compacts prepared by powder sintering. *Scr. Mater.* **2003**, *49*, 1197–1202. [[CrossRef](#)]
36. Fiorilli, S.; Baino, F.; Cauda, V.; Crepaldi, M.; Vitale-Brovarone, C.; Demarchi, D.; Onida, B. Electrophoretic deposition of mesoporous bioactive glass on glass–ceramic foam scaffolds for bone tissue engineering. *J. Mater. Sci. Mater. Med.* **2015**, *26*, 21. [[CrossRef](#)]
37. Du, X.; Yu, B.; Pei, P.; Ding, H.; Yu, B.; Zhu, Y. 3D printing of pearl/CaSO<sub>4</sub> composite scaffolds for bone regeneration. *J. Mater. Chem. B* **2018**, *6*, 499–509. [[CrossRef](#)]
38. Jariwala, S.H.; Lewis, G.S.; Bushman, Z.J.; Adair, J.H.; Donahue, H.J. 3D printing of personalized artificial bone scaffolds. *3D Print. Addit. Manuf.* **2015**, *2*, 56–64. [[CrossRef](#)]
39. Liu, H.; Li, W.; Liu, C.; Tan, J.; Wang, H.; Hai, B.; Cai, H.; Leng, H.-J.; Liu, Z.-J.; Song, C.-L. Incorporating simvastatin/poloxamer 407 hydrogel into 3D-printed porous Ti6Al4V scaffolds for the promotion of angiogenesis, osseointegration and bone ingrowth. *Biofabrication* **2016**, *8*, 045012. [[CrossRef](#)]
40. Hindy, A.; Farahmand, F.; Pourdanesh, F.; Torshabi, M.; Al Janabi, A.H.; Rasoulianboroujeni, M.; Tayebi, L.; Tabatabaei, F.S. Synthesis and characterization of 3D-printed functionally graded porous titanium alloy. *J. Mater. Sci.* **2020**, *55*, 9082–9094. [[CrossRef](#)]
41. Cui, J.; Yi, Y.; Zhang, J.; Chai, L.; Jin, H. Preparation and mechanical properties analysis of porous structure for bone tissue engineering. *Biomed. Mater. Eng.* **2022**, *33*, 465–476. [[CrossRef](#)]
42. Li, B.; Zhang, M.; Lu, Q.; Zhang, B.; Miao, Z.; Li, L.; Zheng, T.; Liu, P. Application and development of modern 3D printing technology in the field of orthopedics. *Biomed Res. Int.* **2022**, *2022*, 8759060. [[CrossRef](#)]
43. Kang, J.; Dong, E.; Li, X.; Guo, Z.; Wang, L. Topological design and biomechanical evaluation for 3D printed multi-segment artificial vertebral implants. *Mater. Sci. Eng. C* **2021**, *127*, 112250. [[CrossRef](#)]
44. Murr, L.E. Metallurgy principles applied to powder bed fusion 3D printing/additive manufacturing of personalized and optimized metal and alloy biomedical implants: An overview. *Prog. Artif. Intell.* **2020**, *9*, 1087–1103. [[CrossRef](#)]
45. Zhang, T.; Zhang, X.; Mao, M.; Li, J.; Sun, H. Chitosan/hydroxyapatite composite coatings on porous Ti6Al4V titanium implants: In vitro and in vivo studies. *J. Periodontal Implant Sci.* **2020**, *50*, 392. [[CrossRef](#)] [[PubMed](#)]
46. Xiao, G.; Yang, L.; Feng, L.; Xinguang, W.; Ke, Z.; Zhongjun, L.; Hua, T. A new 3D printing porous trabecular titanium metal acetabular cup for primary total hip arthroplasty: A minimum 2-year follow-up of 92 consecutive patients. *J. Orthop. Surg. Res.* **2020**, *15*, 383.
47. Sarna-Bo, K.; Skic, K.; Sobieszczański, J.; Boguta, P.; Chaas, R. Contemporary Approach to the Porosity of Dental Materials and Methods of Its Measurement. *Int. J. Mol. Sci.* **2021**, *22*, 8903. [[CrossRef](#)]
48. Bandyopadhyay, A.; Shivaram, A.; Tarafder, S.; Sahasrabudhe, H.; Banerjee, D.; Bose, S. In vivo response of laser processed porous titanium implants for load-bearing implants. *Ann. Biomed. Eng.* **2017**, *45*, 249–260. [[CrossRef](#)]
49. Takahashi, Y.; Tabata, Y. Effect of the fiber diameter and porosity of non-woven PET fabrics on the osteogenic differentiation of mesenchymal stem cells. *J. Biomater. Sci. Polym. Ed.* **2004**, *15*, 41–57. [[CrossRef](#)]
50. Wang, Z.; Wang, C.; Li, C.; Qin, Y.; Zhong, L.; Chen, B.; Li, Z.; Liu, H.; Chang, F.; Wang, J. Analysis of factors influencing bone ingrowth into three-dimensional printed porous metal scaffolds: A review. *J. Alloys Compd.* **2017**, *717*, 271–285. [[CrossRef](#)]
51. Arabi, N.; Zamanian, A.; Rashvand, S.N.; Ghorbani, F. The tunable porous structure of gelatin–bioglass nanocomposite scaffolds for bone tissue engineering applications: Physicochemical, mechanical, and in vitro properties. *Macromol. Mater. Eng.* **2018**, *303*, 1700539. [[CrossRef](#)]
52. Murphy, C.M.; Haugh, M.G.; O'Brien, F.J. The effect of mean pore size on cell attachment, proliferation and migration in collagen-glycosaminoglycan scaffolds for bone tissue engineering. *Biomaterials* **2010**, *31*, 461–466. [[CrossRef](#)]

53. Pei, X.; Wu, L.; Zhou, C.; Fan, H.; Gou, M.; Li, Z.; Zhang, B.; Lei, H.; Sun, H.; Liang, J. 3D printed titanium scaffolds with homogeneous diamond-like structures mimicking that of the osteocyte microenvironment and its bone regeneration study. *Biofabrication* **2020**, *13*, 015008. [[CrossRef](#)] [[PubMed](#)]
54. Zhang, Y.; Sun, N.; Zhu, M.; Qiu, Q.; Zhao, P.; Zheng, C.; Bai, Q.; Zeng, Q.; Lu, T. The contribution of pore size and porosity of 3D printed porous titanium scaffolds to osteogenesis. *Biomater. Adv.* **2022**, *133*, 112651. [[CrossRef](#)] [[PubMed](#)]
55. Li, H.; Yao, B.; Li, Z.; Peng, Y.; Fan, H. Compressive properties and deformation mechanism of selective laser melting of Ti6Al4V porous femoral implants based on topological optimization. *Compos. Struct.* **2023**, *321*, 117326. [[CrossRef](#)]
56. Tan, C.; Zou, J.; Li, S.; Jamshidi, P.; Abena, A.; Forsey, A.; Moat, R.J.; Essa, K.; Wang, M.; Zhou, K. Additive manufacturing of bio-inspired multi-scale hierarchically strengthened lattice structures. *Int. J. Mach. Tools Manuf.* **2021**, *167*, 103764. [[CrossRef](#)]
57. Ahmadi, S.M.; Amin Yavari, S.; Wauthle, R.; Pouran, B.; Schrooten, J.; Weinans, H.; Zadpoor, A.A. Additively manufactured open-cell porous biomaterials made from six different space-filling unit cells: The mechanical and morphological properties. *Materials* **2015**, *8*, 1871–1896. [[CrossRef](#)] [[PubMed](#)]
58. Herrera, A.; Yáñez, A.; Martel, O.; Afonso, H.; Monopoli, D. Computational study and experimental validation of porous structures fabricated by electron beam melting: A challenge to avoid stress shielding. *Mater. Sci. Eng. C* **2014**, *45*, 89–93. [[CrossRef](#)] [[PubMed](#)]
59. Jahir-Hussain, M.J.; Maaruf, N.A.; Esa, N.E.F.; Jusoh, N. The effect of pore geometry on the mechanical properties of 3D-printed bone scaffold due to compressive loading. *IOP Conf. Ser. Mater. Sci. Eng.* **2021**, *1051*, 012016. [[CrossRef](#)]
60. Van Bael, S.; Chai, Y.C.; Truscello, S.; Moesen, M.; Kerckhofs, G.; Van Oosterwyck, H.; Kruth, J.-P.; Schrooten, J. The effect of pore geometry on the in vitro biological behavior of human periosteum-derived cells seeded on selective laser-melted Ti6Al4V bone scaffolds. *Acta Biomater.* **2012**, *8*, 2824–2834. [[CrossRef](#)]
61. Xu, J.; Weng, X.-J.; Wang, X.; Huang, J.-Z.; Zhang, C.; Muhammad, H.; Ma, X.; Liao, Q.-D. Potential use of porous titanium–niobium alloy in orthopedic implants: Preparation and experimental study of its biocompatibility in vitro. *PLoS ONE* **2013**, *8*, e79289. [[CrossRef](#)]
62. Danlei, Z.; Yutian, H.; Yong, A.; Changjun, H.; Qian, W.; Yan, L.; Jie, L.; Qingsong, W.; Zhen, Z. Effect of pore geometry on the fatigue properties and cell affinity of porous titanium scaffolds fabricated by selective laser melting. *J. Mech. Behav. Biomed. Mater.* **2018**, *88*, 478–487.
63. Kovács, Á.É.; Csernátóny, Z.; Csámer, L.; Méhes, G.; Szabó, D.; Veres, M.; Braun, M.; Harangi, B.; Serbán, N.; Zhang, L. Comparative analysis of bone ingrowth in 3D-printed titanium lattice structures with different patterns. *Materials* **2023**, *16*, 3861. [[CrossRef](#)]
64. Lim, H.-K.; Ryu, M.; Woo, S.-H.; Song, I.-S.; Choi, Y.-J.; Lee, U.-L. Bone conduction capacity of highly porous 3D-printed titanium scaffolds based on different pore designs. *Materials* **2021**, *14*, 3892. [[CrossRef](#)]
65. Farazin, A.; Zhang, C.; Gheisizadeh, A.; Shahbazi, A. 3D bio-printing for use as bone replacement tissues: A review of biomedical application. *Biomed. Eng. Adv.* **2023**, *5*, 100075. [[CrossRef](#)]
66. Deng, F.; Liu, L.; Li, Z.; Liu, J. 3D printed Ti6Al4V bone scaffolds with different pore structure effects on bone ingrowth. *J. Biol. Eng.* **2021**, *15*, 4. [[CrossRef](#)]
67. Huang, G.; Pan, S.-T.; Qiu, J.-X. The osteogenic effects of porous Tantalum and Titanium alloy scaffolds with different unit cell structure. *Colloids Surf. B* **2022**, *210*, 112229. [[CrossRef](#)]
68. Yan, Y.; Kang, Y.; Li, D.; Yu, K.; Zhang, Y. Microstructure, mechanical properties and corrosion behavior of porous Mg-6wt.% Zn scaffolds for bone tissue engineering. *J. Mater. Eng. Perform.* **2018**, *27*, 970–984. [[CrossRef](#)]
69. Wang, C.; Xu, D.; Lin, L.; Li, S.; Hou, W.; He, Y.; Sheng, L.; Yi, C.; Zhang, X.; Li, H. Large-pore-size Ti6Al4V scaffolds with different pore structures for vascularized bone regeneration. *Mater. Sci. Eng. C* **2021**, *131*, 112499. [[CrossRef](#)] [[PubMed](#)]
70. Song, C.; Liu, L.; Deng, Z.; Lei, H.; Yuan, F.; Yang, Y.; Li, Y.; Yu, J. Research progress on the design and performance of porous titanium alloy bone implants. *J. Mater. Res. Technol.* **2023**, *23*, 2626–2641. [[CrossRef](#)]
71. Karageorgiou, V.; Kaplan, D. Porosity of 3D biomaterial scaffolds and osteogenesis. *Biomaterials* **2005**, *26*, 5474–5491. [[CrossRef](#)] [[PubMed](#)]
72. Taniguchi, N.; Fujibayashi, S.; Takemoto, M.; Sasaki, K.; Otsuki, B.; Nakamura, T.; Matsushita, T.; Kokubo, T.; Matsuda, S. Effect of pore size on bone ingrowth into porous titanium implants fabricated by additive manufacturing: An in vivo experiment. *Mater. Sci. Eng. C* **2016**, *59*, 690–701. [[CrossRef](#)] [[PubMed](#)]
73. Guo, A.X.; Cheng, L.; Zhan, S.; Zhang, S.; Xiong, W.; Wang, Z.; Wang, G.; Cao, S.C. Biomedical applications of the powder-based 3D printed titanium alloys: A review. *J. Mater. Sci. Technol.* **2022**, *125*, 252–264. [[CrossRef](#)]
74. Hara, D.; Nakashima, Y.; Sato, T.; Hirata, M.; Kanazawa, M.; Kohno, Y.; Yoshimoto, K.; Yoshihara, Y.; Nakamura, A.; Nakao, Y. Bone bonding strength of diamond-structured porous titanium-alloy implants manufactured using the electron beam-melting technique. *Mater. Sci. Eng. C* **2016**, *59*, 1047–1052. [[CrossRef](#)] [[PubMed](#)]
75. Zhou, C.; Ye, X.; Fan, Y.; Ma, L.; Tan, Y.; Qing, F.; Zhang, X. Biomimetic fabrication of a three-level hierarchical calcium phosphate/collagen/hydroxyapatite scaffold for bone tissue engineering. *Biofabrication* **2014**, *6*, 035013. [[CrossRef](#)] [[PubMed](#)]
76. Ran, Q.; Yang, W.; Hu, Y.; Shen, X.; Yu, Y.; Xiang, Y.; Cai, K. Osteogenesis of 3D printed porous Ti6Al4V implants with different pore sizes. *J. Mech. Behav. Biomed. Mater.* **2018**, *84*, 1–11. [[CrossRef](#)] [[PubMed](#)]
77. Wang, C.; Wu, J.; Liu, L.; Xu, D.; Liu, Y.; Li, S.; Hou, W.; Wang, J.; Chen, X.; Sheng, L. Improving osteoinduction and osteogenesis of Ti6Al4V alloy porous scaffold by regulating the pore structure. *Front. Chem.* **2023**, *11*, 1190630. [[CrossRef](#)] [[PubMed](#)]

78. Ouyang, P.; Dong, H.; He, X.; Cai, X.; Wang, Y.; Li, J.; Li, H.; Jin, Z. Hydromechanical mechanism behind the effect of pore size of porous titanium scaffolds on osteoblast response and bone ingrowth. *Mater. Des.* **2019**, *183*, 108151. [[CrossRef](#)]
79. Wei, X.; Tang, Z.; Wu, H.; Zuo, X.; Dong, H.; Tan, L.; Wang, W.; Liu, Y.; Wu, Z.; Shi, L. Biofunctional magnesium-coated Ti6Al4V scaffolds promote autophagy-dependent apoptosis in osteosarcoma by activating the AMPK/mTOR/ULK1 signaling pathway. *Mater. Today Bio* **2021**, *12*, 100147. [[CrossRef](#)] [[PubMed](#)]
80. Qiao, S.; Wu, D.; Li, Z.; Zhu, Y.; Zhan, F.; Lai, H.; Gu, Y. The combination of multi-functional ingredients-loaded hydrogels and three-dimensional printed porous titanium alloys for infective bone defect treatment. *J. Tissue Eng.* **2020**, *11*, 2041731420965797. [[CrossRef](#)]
81. Wang, C.; Liu, D.; Xie, Q.; Liu, J.; Deng, S.; Gong, K.; Huang, C.; Yin, L.; Xie, M.; Guo, Z. A 3D printed porous titanium alloy rod with diamond crystal lattice for treatment of the early-stage femoral head osteonecrosis in sheep. *Int. J. Med. Sci.* **2019**, *16*, 486. [[CrossRef](#)]
82. Zhang, C.; Zhang, L.; Liu, L.; Lv, L.; Gao, L.; Liu, N.; Wang, X.; Ye, J. Mechanical behavior of a titanium alloy scaffold mimicking trabecular structure. *J. Orthop. Surg. Res.* **2020**, *15*, 40. [[CrossRef](#)]
83. Li, P.; Jiang, W.; Yan, J.; Hu, K.; Han, Z.; Wang, B.; Zhao, Y.; Cui, G.; Wang, Z.; Mao, K. A novel 3D printed cage with microporous structure and in vivo fusion function. *J. Biomed. Mater. Res. Part A* **2019**, *107*, 1386–1392. [[CrossRef](#)] [[PubMed](#)]
84. Gao, H.; Li, X.; Wang, C.; Ji, P.; Wang, C. Mechanobiologically optimization of a 3D titanium-mesh implant for mandibular large defect: A simulated study. *Mater. Sci. Eng. C* **2019**, *104*, 109934. [[CrossRef](#)] [[PubMed](#)]

**Disclaimer/Publisher's Note:** The statements, opinions and data contained in all publications are solely those of the individual author(s) and contributor(s) and not of MDPI and/or the editor(s). MDPI and/or the editor(s) disclaim responsibility for any injury to people or property resulting from any ideas, methods, instructions or products referred to in the content.